Nanoscale

Accepted Manuscript

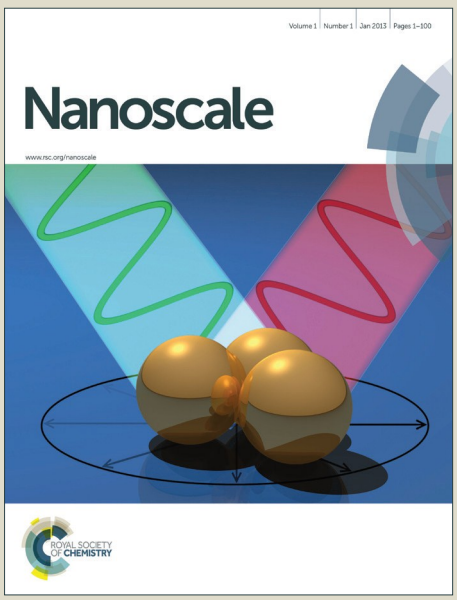

ROYAL SOCIETY OF CHEMISTRY

www.rsc.org/nanoscale

Hybrid light sensor based on ultrathin Si nanomembranes sensitized with CdSe/ZnS colloidal nanocrystal quantum dots

Weina Peng[1], Siddharth Sampat[2], Sara M. Rupich[1], Benoy Anand[2], Hue Minh Nguyen[2*], David Taylor[2], Brandon E. Beardon[1], Yuri N. Gartstein[2], Yves J. Chabal[1] and Anton V. Malko[2]

[1]Department of Materials Science and [2]Department of Physics, The University of Texas at Dallas, Richardson, TX, 75080

Abstract

We report the observation of a large enhancement of the wavelength-dependent photocurrent in ultrathin silicon nanomembranes (SiNM) decorated with colloidal CdSe/ZnS nanocrystal quantum dots (NQDs). Back-gated, field-effect transistor structures based on 75 nm-thick SiNMs are functionalized with self-assembled monolayers (SAMs) preventing surface oxidation and minimizing the surface defect densities. NQDs are drop cast on the active region of the device and the photocurrent is measured as a function of the excitation wavelength across the NQD absorption region. Photocurrent enhancement on the order of several hundred nA's is observed for NQD/SAM/SiNM devices compared to reference SAM/SiNM structures, with the device peak response closely correlated to the QD absorption peak. We propose light-induced gating of the surface electrostatic potential and forward self-biasing of the FET channel as the two key mechanisms leading to the large photocurrent increase. Our findings open the possibility of employing silicon-nanocrystal hybrid structures for light sensing applications.

* Current address: Center for Integrated Nanotechnologies, Los Alamos National Laboratory, Los Alamos, NM, 87545

Hybrid nanostructured materials have attracted significant attention for their potential in the development of a new generation of optoelectronic devices including light sensors and photovoltaic devices. Low cost, high-sensitivity photodetectors with wide spectral response also have important applications in remote sensing, biomedical detection and imaging. Since their introduction in the past several decades, colloidal semiconductor nanocrystal quantum dots (NQDs) have offered an attractive potential for enhancing photon detection capabilities due to their bandgap tunability and ease of manufacture and processing. Highly sensitive photodetectors based on colloidal NQD solids exhibiting carrier mobilities in the range 10^{-3} -10^{-2} cm^2 V^{-1} s^{-1} and photoconductive gains in the range 10-100 have been reported.[1]

Photoconductive detectors based on solution processable light absorbers such as colloidal NQDs or dye sensitizers mostly rely on exciton dissociation within the bulk heterojunction or at the interfaces between the layers and subsequent charge transport through the entire film thickness. As the result, their performance is often limited, stemming from the insufficient charge carrier mobility and the deleterious effects of interface states known to trap carriers.[2] Alternatively, several publications have reported the use of colloidal NQDs as a light activated gate for thin-film field effect transistors made from epitaxially grown GaAs/AlGaAs structures.[3,4] For these devices, the charge transport takes place within the underlying semiconductors with much higher electron and hole mobility. Recently, an emerging class of atomically thin materials, such as transition metal dichalcogenide (TMDC) materials (most notably MoS_2), have shown promise in the development of the high gain photodetectors.[5]

Here, we present light sensing hybrid device based on a back-gated, ultrathin (75 nm) Si nanomembrane (SiNM) field effect transistor (FET) sensitized with CdSe/ZnS colloidal NQDs, as schematically shown in Fig 1(a). A self-assembled monolayer (SAM) is used to passivate the

SiNM surface and reduce the number of interface trapping centers[6,7,8] that are known to adversely affect FET performances. CdSe/ZnS NQDs are then drop-cast on the surface of the SAM/SiNM device with a 20μm × 20μm active region and shown to form a thin (<100 nm) film of NQDs with the majority accumulating in trenches that appear unintentionally during HF etching at the doped/undoped junction in the vicinity of the source and drain contacts. When illuminated with a laser, a large current is observed with a magnitude that is several hundred nA's in the NQD/SAM/SiNM device compared to ~nA's for the SAM/SiNM FET (no NQD deposition) reference structure. The photocurrent enhancement observed as a function of the excitation wavelength follows the optical absorption profile of the deposited NQDs, suggesting that the photocurrent is nanocrystal-related. The observed photoresponse of NQD/SAM/SiNM FET devices (peak value of ~0.1 A/W) vs. the reference SAM/SiNM FET device exhibit high gain values up to 300.

Back-gated field-effect transistors are fabricated on silicon-on-insulator (SOI) substrates (p-type, nominal doping 10^{15} cm^{-3}, 3 μm buried oxide, purchased from Soitec). The device schematic is shown in Fig. 1(a) and a microscopic image of the channel region after the completion of device fabrication is shown in Fig. 1(b). The thickness of the Si layer is reduced from 300 nm down to ~75 nm using repeated oxidation and oxide removal with HF. The undoped channel in the SiNM region is a 20 μm × 20 μm square and the adjacent regions are doped with Boron via ion implantation (doping ~ 1×10^{20} cm^{-3}) to achieve good ohmic contact. The doped and undoped regions have a visible color contrast and can be easily distinguished in the optical images. Metal Cr/Au contacts are then deposited using e-beam evaporation with metal lift-off processes as seen in Fig. 1(b). The Cr/Au metal stack is chosen as it is compatible with the wet chemistry processing necessary for SAM functionalization. The Si membrane surface is

then terminated with ester groups according to a previously established method.[9] The SAM/Si interface is known to have a very low interface defect density (~ 10^{11} $cm^{-2}eV^{-1}$) [7,8] leading to an extremely slow surface recombination velocity (~20 cm/s).[10] More importantly, the versatile functionality of SAM fosters controlled deposition of NQDs in uniform 2D layers and can be further extended to 3D multilayers.[11] Although, in our current study the SAM layer serves mainly as the surface passivating layer and controlled spacer, we proceed with this hybrid structure for further exploitation of the unique SAM/NQD system.

In the course of this surface investigation of the SAM functionalized devices, we have found that groves are unintentionally etched at each end of the channel as seen Fig. 1(c). The grooves only form in the presence of gold during HF etching step via metal assisted chemical etching (MACE).[12] However, this step is required to prepare a hydrogen terminated Si surface for the hydrosilylation reaction. AFM profiles (Fig. 1(d)) reveal that the groves form in the undoped region at the doped/undoped boundary as confirmed by the fact that the inter-groove distance is exactly 20 μm corresponding to the width of the active region. Each grove is ~ 2 μm wide (the width varies depending on the etching time and HF concentration) and is characterized by a depth that can in some cases be as large as the thickness of the Si nanomembrane (~ 75nm) but typically ~0.6-0.7 of that depth. CdSe/ZnS NQDs (Life Technologies, P/N Q21711MP and Q21701MP, peak emissions at 585 nm (NQD-585) and 605 nm (NQD-605), respectively, 4 μM stock solutions) are drop-cast from a 9:1 hexane:octane solution onto the functionalized SiNM surface and have a tendency to accumulate inside the grooves. We observed a closely packed and nearly continuous NQDs film (several monolayers thick) formed at the membrane surface with higher NQD concentrations within the grooves as confirmed by SEM imaging and EDAX profiling shown in Suppl. Info Fig S1. For the excitation wavelength-resolved photocurrent

measurements, a white-light supercontinuum emission is employed (NewPort SCG-800 Photonic Crystal Fiber) in a manner similar to the one described in Ref [13]. A narrow spectral bandwidth is selected with a bandpass filter (~10 nm), set to a low optical power ensuring the NQDs are excited in the linear optical response regime. The laser beam is then focused with a low magnification objective onto the device active region that is kept under vacuum (base pressure ~ 10^{-6} -10^{-7} Torr) in a cryostat. The laser spot profile is Gaussian with a 25 - 30 μm diameter, illuminating the entire channel region. The photocurrent is recorded using an HP4155 semiconductor parameter analyzer.

Fig. 2 (a) shows the typical behavior of the source-drain current I_d as a function of the gate voltage V_g for the reference SiNM FET device both in the dark and under laser illumination. A constant drain voltage V_{ds} = 10 V is applied to the drain contact and the source contact remains grounded during the entire measurement. The device performance under dark conditions exhibits a characteristic FET behavior: a conductive channel is formed under large negative gate bias and an insignificant off current (<100 pA) is observed through the channel as V_g is increased above zero gate voltage. A large gate voltage sweep ($-50V \leq V_g \leq 50V$) is necessary to modulate the device between "ON" and "OFF" behavior as a consequence of the thick (3μm) buried oxide in the SOI structure. Although the channel is *p*-doped, it has been shown that the bulk doping level is irrelevant for thin Si nanomembranes[14,15] as the interface-states effects prevail. The subthreshold slope extracted from the dark current is 2 – 6 V/decade for the reference devices, corresponding to an interface trap density D_{it} ~ (2 – 7)×10^{11} $cm^{-2}eV^{-1}$. This number is in good agreement with the previous studies on the defect characterization of the SAM/Si interfaces using conductance voltage measurements. [7,8] It needs to be kept in mind, however, that the D_{it} at the buried oxide interface also contributes to the device subthreshold swing for these devices.[15]

The low observed D_{it} confirms the effective passivation of both surfaces by forming gas annealing of the buried oxide interface (performed before Cr/Au deposition) and SAM passivation of the top surface.

Upon illumination, the I_d-V_g curve exhibits a prominent change in the dark current "OFF" regime. The region between V_g = 0 and 10 V shows a slowly varying photocurrent response as a function of gate voltage. At the beginning of this region, defined as the transition point, the current linearly increases with the excitation power (see inset of Fig. 2(a)) and the intercept passes close to zero, indicating that it is dominated by the photocurrent (i.e. results from photoexcitation). This property provides a reference point for the direct comparison of device behavior before and after NQD deposition.

Fig. 2 displays the I_d-V_g curves as a function of the excitation wavelength for the SAM-passivated devices (SAM/Si are shown in Fig 2(b) and those of the same device coated with a NQD-585 layer (NQD/SAM/Si) are given in Fig. 2(c)) for an optical power of 20 μW at each wavelength. Similar to Fig. 2(a), a fairly flat photocurrent region is observed in both graphs, although the absolute dependence of the photocurrent differs from that in Fig. 2(a). After the deposition of QDs, a clear change in wavelength-dependent photoresponse indicated by I_d is observed while the dark current behavior remains largely unchanged. However, I_d does not show a constant response in the photocurrent dominant region and gradually decreases as V_g increases (i.e. goes to higher positive values). In general, the magnitude of the photocurrent depends on several factors, particularly carrier mobility and lifetime. Both factors are a complex function of the gate voltage since interface scattering at the device surface plays an important role in the carrier transport and surface recombination dominates the bulk recombination in these ultra-thin Si films with a low doping level. It is clear from Figure 2 that the V_g variation is crucial in

determining the transition point as the transition point shifts by more than 20 V after NQD deposition. Among all the devices measured, a shift of the device dark response, up to ± 25 V, has been observed after the NQD deposition. This voltage shift of the device dark current is similar to the threshold voltage shift observed in chemical sensors when charged molecules are absorbed onto the sensor surface, suggesting that this shift originates from changes in local electrostatic environment at the device surface.[16]

A detailed understanding of I_d-V_g behavior in surface-functionalized thin SOI FET structures requires a 2D simulation (electrical field distribution both vertically and longitudinally) incorporating parameters that describe both surface scattering and surface recombination, and is currently under investigation. However, the transition point conveniently defines the beginning of the flat region in the photocurrent response and therefore is used as the reference for comparison of photocurrent values at different wavelengths and optical powers. Hence, the control of the back gate voltage becomes essential in order to locate the transition point accurately. The photocurrent at the transition point is plotted in Fig. 3 as a function of the excitation wavelength for the NQD/SAM/SiNM devices. For the SAM/SiNM devices before sensitization with NQDs, the photocurrent level is below 30 nA for all the devices measured (Supporting Information, Fig. S2). Fig. 3 (a) shows photocurrent for NQD-585/SAM/SiNM device with data extracted from Fig. 2 (c), and Fig. 3 (b) shows the data for NQD-605/SAM/SiNM device (original source-drain I_d-V_g current graphs are similar and not shown). The photocurrents increase 1 -2 orders of magnitude as compared to the reference SAM/SiNM structures and have a clear wavelength dependence, peaking close to the absorption maxima of each type of NQDs. The distinct peak position for the two types of NQDs is a clear proof of the NQD-related origin of the photocurrent.

In order to understand the photocurrent enhancement we considered two mechanisms: i) change in the electrostatic potential of the channel surface and ii) forward biasing of the junction by the minority carriers that leads to the current gain and amplification facilitated by the trench geometry. For the first mechanism, the number of photoexcited excitons produced in both the NQD layer and the Si nanomembrane are estimated and compared with the observed values of the photocurrent. The silicon absorption monotonically varies in the region between 500-700 nm as seen in Supp. Info, Fig. S2. Considering a SiNM with thickness of *t=75 nm*, the direct Si absorption is estimated to be 11- 12% over the wavelength region. Assuming 100% charge collection efficiency within the entire SiNM active region, one would obtain photocurrents on the order of 200-800 nA in bare SAM/SiNM structures. While the photocurrent in all of the SAM/SiNM devices follows the Si absorption curve (Supp. Info, Fig. S2), the maximum observed values are only ~30 nA indicating lower collection efficiency within the undoped Si NM itself. The drain-voltage dependence (Suppl. Info, Fig. S3) exhibits a small current change with the increasing drain voltage when V_d is larger than several volts. This suggests that the observed photocurrent is likely to have a large diffusion component instead of being dominated by drift current. Therefore, a relevant factor here is the minority carrier diffusion length L_D, which determines how far electrons and holes can travel without recombination. Surface recombination significantly reduces the carrier life time for our thin SiNMs. The bulk carrier lifetime τ_b of Si is around 10-100 μs[17] for a doping level of 10^{15} cm^{-3}. With surface recombination velocity of 100 cm/s[18] for D_{it} on the order of 10^{11} ~ 10^{12} $cm^{-2}eV^{-1}$, the carrier lifetime is reduced to approximately 0.04 μs. Consequently, the minority carrier diffusion length is estimated to be less than 5 μm, much smaller than the channel length (20 μm). As the result, the photoexcited carriers are only collected in the regions close to contacts. For *p-i-n* devices

based on SiNMs of the same thickness (Supp. Info, Fig. S4), we observed the minority carrier diffusion length L_D to be less than 4 μm.

Under such conditions, only the contribution from NQDs that accumulate in the trenches or close to the contact regions (Fig. 1 (c, d)) can influence the photocurrent either via charge (CT) or energy (ET) transfer of photoexcited carriers from NQDs to SiNM. However, due to the relatively small absolute amount of NQDs within the trenches (since their depth is only ~50 nm and width ~2 μm), the NQDs direct contribution to the photocurrent is expected to be fairly small. Indeed, microPL spectra taken in the vicinity of trenches (with probing spot diameter <1 μm) show average PL counts correspond to ~10's of NQDs layers when compared with previously measured PL intensity level from a single NQD monolayer grafted on bare Si.[19] The linear absorption coefficient of NQD films has been estimated to be in the range of $(1\text{-}2)\times10^4$ cm^{-1} at 550 nm, which is comparable to the Si absorption at this wavelength. Thus, 10 ~ 15 monolayers of NQDs, which are approximately 50 ~ 75 nm thick, absorb approximately the same amount of photon energy as the SiNMs. Even if all of the photoexcited carriers generated within the NQD film inside 2μm-deep trenches were directly transferred to the SiNM without any loss, either via charge or energy transfer, the additional photocurrent would likely only be < 40 nA - a level comparable to bare SAM/SiNM devices.

At this point, we are not able to accurately determine the individual contributions of charge (CT) and energy (ET) transfer mechanisms to the entire carrier transport. In NQDs with strong surface trapping, excitons indeed dissociate at the surface, thus producing separated electrons and holes, and providing mobile charge carriers. However, since the NQD film structure has not been optimized, the carrier diffusion length will likely not exceed ~10-20 nm

because of the insulating organic ligands between neighboring NQDs and thus only layers immediately adjacent to the SiNM surface may add to the photocurrent due to CT. On the other hand, we have recently shown that non-radiative (NRET) and radiative (RET) energy transfer mechanisms are able to electromagnetically couple photoexcited excitons across the interface into Si substrate with efficiencies close to 90 % for NQD mono- and bilayers.[11,20,21,22] Still, this mechanism cannot directly account for the observed levels of photocurrent in NQD/SAM/Si devices due to the limited absorption in the NQDs as discussed previously.

The existence of trenches at the border of doped/undoped region of SiNM is an important factor in the performance of the devices. SiNMs terminated with native oxide layer (~ 2 nm) instead of SAM had no such trenches due to the absence of HF etching. The performance of these devices (Suppl. Info, Fig. S5) is reproducible with little variation across several devices and the photocurrent levels are on the order of 10 nA under 512 nm laser illumination across the range of similar V_g values. Further, when NQDs are added onto the surface of oxide-terminated Si NMs, the photocurrent remains essentially unchanged (within approx. 30% device-to-device variation). However, when trenches were intentionally formed at the border of the doped/undoped regions of oxide-terminated SiNMs, a photocurrent increase was observed upon the addition of NQDs (Suppl. Info, Fig. S6). In that case, the current enhancement was smaller as a result of the limited precision of lithographic patterning, with the location of trenches 350 nm into the doped region.

According to the recently published work,[3,4] NQDs were placed on SAM-passivated GaAs surfaces and observed to act as a light-activated gate via the change in the electrochemical potential following the light absorption. This suggests that, upon photoexcitation, charge transfer may occur within the NQD layer leading to an accumulation of charges in the organic ligands

that passivate NQDs. This leads to a change in the electrostatic potential between the NQD layers and the semiconductor transistor conducting channel. Hence, the FET works as an amplifier and the change in the channel current can be much larger than the number of photoexcited excitons in the NQDs.. A similar principle had previously been applied in chemical sensing devices.[23] This should be contrasted with a more conventional, light absorption/charge transfer-based photocurrent sensing modality more common with colloidal nanocrystals.[24] In our devices, NQDs located in the trenches are in a direct contact with the FET short conductive channels, further affecting the electrostatic potential. This point of view is corroborated by the noticeable shift of the I_d–V_g curves and the corresponding transition points upon NQD's addition, as previously shown in Fig. 2 (b) and (c).

The second mechanism that can explain the observed increase in the FET photocurrent is forward self-biasing and current amplification under illumination in short channel SOI-FET structures.[25] When the channel is depleted (e.g., at the transition point), there exists large band bending at both the source and the drain junctions as schematically shown in Fig. 3(c). Upon illumination, photoexcited NQD excitons can be non-radiatively and radiatively transferred to an adjacent Si channel in the vicinity of the junctions. The band bending near the source side favors hole collection while electrons remain in the channel as the band bending at the drain side is in the opposite direction to electron diffusion. Electrons accumulating in the channel self-bias forward the drain junction and lead to a reduction in the barrier height at the drain side which is observed as an increase in electron diffusion from the channel to the drain contact. Meanwhile, this self-biasing effect generates a larger hole diffusion current from the drain contact to the channel due to the higher doping level of the drain. This facilitates a large hole-dominated gain (G) and amplification of the total photocurrent. For instance, Yamamoto et al.[2525] have shown

very sensitive SOI photodetectors with gain factors ranging from G~1 to G~50 for SOI FETs with channel length varying from 20 to 1 μm (channel thickness 170 nm). In this case, those devices were on bare SiNM, without application of any photosensitizers, and with light absorption taking place in SiNM alone. However, their findings support our observation that trenches play an important part in the amplification process by forming short channel regions (trench width ~2 μm) that are within the diffusion length L_D < 4 μm for efficient charge collection. NQDs that accumulate inside the trenches play dominant role in the current amplification as compared to the ones on the flat region of the device due to more efficient CT/ET of the photoexcited excitons in the junction regions. This may explain the amplification levels shown for the device in Fig. 3 (a) with gain values G_{585} ~275. The observed current levels up to 200 nA at the peak NQD absorption wavelength greatly exceed those found in the bare SiNMs structures under similar excitation conditions.[25] The wavelength-dependent photoresponse of the NQD/SAM/SiNM devices taking into account the illuminated area of the trenches (length 15 μm, width ~2 μm) is approximately 0.04 - 0.1 A/W in the region between 700-500 nm, as shown on right scale of Fig. 3 (a) and (b). These values are comparable to the performance of the commercial photodetectors (~0.5-0.7 A/W) despite very thin SiNM and extremely small amount of photosensitizer NQDs employed on the substrate. Further improvement in photoresponse can possibly be obtained by employing optically dense, multilayer NQD films assembled on Si nanowire geometries[26] that are several microns long with gradient size distribution for efficient directed energy transfer[11] towards the conducting nanowires. The use of Si nanowire geometry will help to separate optical and electrical pathways – absorption of the incoming sunlight occurs in the vertical direction, while ET will preferentially happen in the horizontal plane. Nanowire structures can be fabricated to be thin

(down to 50 nm diameter) and closely spaced (center to center spacing ~ 150 nm), thus allowing dense NQD packing and proximity to Si. Such Si nanoscaffolds can certainly be used with other types of photosensitizers, including infrared active NQDs with absorption close to 1 μm.

In summary, we have prepared back-gated Si-nanomembrane FET devices functionalized with SAM and deposited thin layers of CdSe/ZnS nanocrystals by drop-coating. We observe a large photocurrent increase of several hundred nAs in NQD/SAM/SiNM compared to ~nAs levels in reference SAM/SiNM structures without NQDs. The observed photocurrent has a clear excitation-wavelength dependence that follows the NQD absorption profile, thus confirming its NQD-related origin. We observe that the presence of unintentional trenches at the border of the doped/undoped regions of the SiNM during the substrate preparation plays a crucial role in the photocurrent amplification. We propose two possible mechanisms to explain the observed large photocurrent increase: i) change in the electrostatic potential of the channel surface and ii) forward biasing of the junction by the minority carriers that leads to the current gain and amplification facilitated by the trench geometry. The observed photocurrent gain values approach 0.1 A/W at the peak wavelength, comparable to the performance of the commercial bulk Si photodetectors despite the ultrathin Si nanomembrane thickness. These proof-of-concept results are very encouraging for the further development of the sensitive and versatile photodetectors by incorporating easily processable semiconductor NQDs with wide spectral response to the existing commercial Si technology.

This work was supported by the U.S. Department of Energy, Office of Science, Basic Energy Sciences, under Award # DE-SC0010697. The subtask of development by WP of the electrical measurement technique and associated cells was supported by NSF (CHE-1300180).

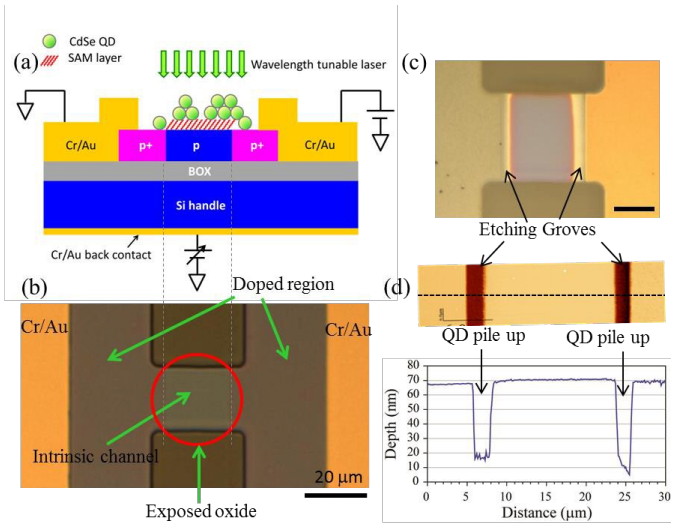

FIG. 1 (a) Schematic cross-section view of the FET device used for photocurrent measurements. The device is fabricated on SOI substrates (70 nm Si and 3 μm buried oxide (BOX)). Both source and drain contacts are highly doped with Boron (~ 10^{20} cm^{-3}) and metalized with 10 nm Cr/90 nm Au. The same metal combination is used to make the back side contact. (b) Optical microscopic image of the channel region before hydrosilyation. The channel is 20 μm long and 20 μm wide. The doped and the undoped region can be distinguished by the color difference. The red circle indicates the position and the size of the laser excitation, which covers the entire active region. (c) An optical microscopic image of the device after SAM functionalization. Two etching groves at the doped/undoped boundary are visible. The scale bar is 10 μm. (d) AFM image of the center of the device (7 μm × 30 μm) and height profile along the dashed line.

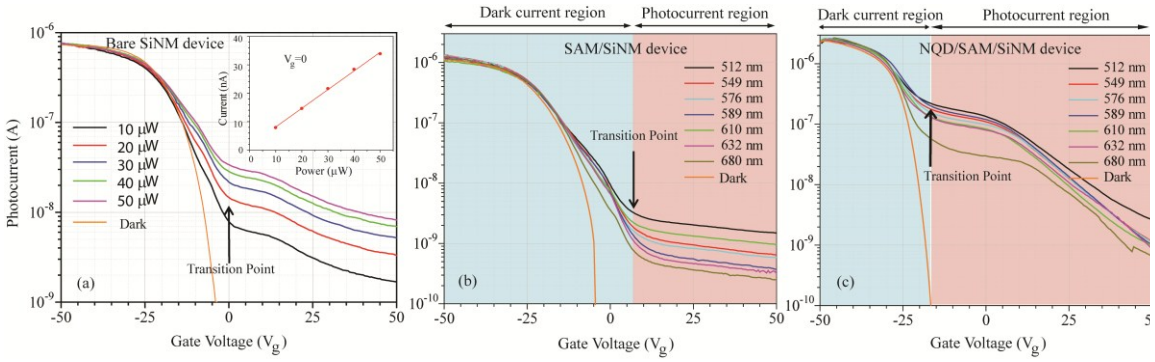

FIG. 2 (a) Photocurrent as a function of the back gate voltage for the bare Si device at different optical excitation powers. Excitation wavelength 512 nm. Inset: photocurrent at the transition point as a function of the optical power. Photocurrents as a function of the back gate voltage for different excitation wavelengths (b) for a SAM/SiNM device and (c) for a NQD/SAM/SiNM device. The device dark current behavior is shown for comparison in each panel. The transition point at the beginning of the photocurrent dominant region (indicated by the arrows) is used to examine the effects when NQDs are added to the system.

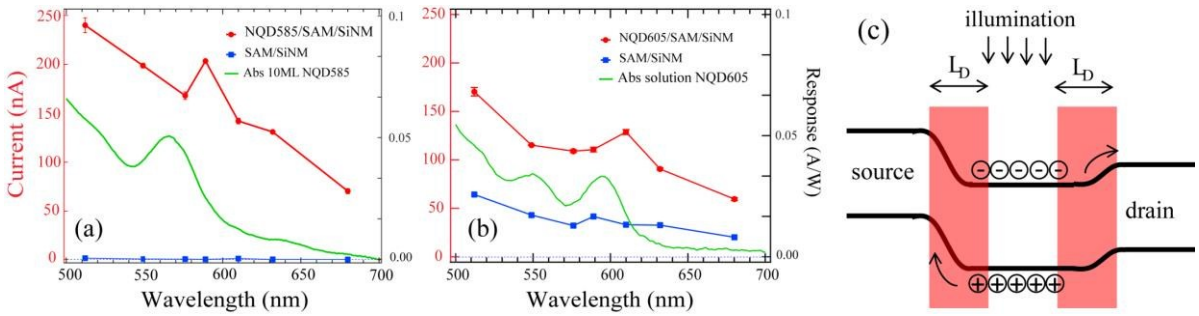

FIG. 3 (a) Red trace - photocurrent as a function of the excitation wavelength in NQD-585/SAM/SiNM device. Blue trace – photocurrent in SAM/SiNM only device before deposition of NQDs. Error bars indicate variations from several consecutive measurements. Lines connecting experimental data points (red and blue) are guides for the eye only. Green curve – absorption of the NQD-585 10 monolayer sample on glass substrate (b) Same measurements for the photocurrent in NQD-605/SAM/SiNM sample (red), in SAM/SiNM only sample (blue) and absorption of NQD-605 in solution (green). (c) Band diagram of the FET device in the dark current "OFF" region. The device manifests a self-biasing effect, leading to current amplification. The red region indicated the minority carrier diffusion length (2 ~ 4 μm for thin SiNMs).

[1] Mcdonald S. A., Konstantatos G., Zhang S., Cyr P. W., Klem E. J. D., Levina L. and Sargent E. H., "Solution-processed PbS quantum dot infrared photodetectors and photovoltaics", *Nature Materials* **2005**, *4*, 138 - 142

[2] Greenham N.C.; Peng X.;, and Alivisatos A.P., "Charge separation and transport in conjugated polymer/semiconductor-nanocrystal composites studied by photoluminescence quenching and photoconductivity." *Phys. Rev. B* **1996**, *54 (24)*, 17628

[3] Aqua T.; Naaman R.; Aharoni A.; Banin U.; and Paltiel Y., "Hybrid nanocrystals-organic –semiconductor light sensor", *Appl. Phys. Lett.* **2008**, *92*, 223112

[4] Y. Paltiel, A. Aharoni, U. Banin, O. Neuman and Y. R. Naaman, "Self-Assembling of InAs Nanocrystals on GaAs: The Effect of Electronic Coupling and Embedded Gold Nanoparticles on the Photoluminescence" *Appl. Phys. Lett.* **2006**, ***89***, 033108

[5] Kufer D.; Nikitskiy I.; Lasanta T.; Navickaite G.; Koppens F. H. L.; and Konstantos G., "Hybrid 2D–0D MoS_2 – PbS Quantum Dot Photodetectors" *Adv. Mat.* **2015**, *27*, 176-180

[6] Aureau D.; Varin Y.; Roodenko K.; Seitz O.; Pluchery O.; and Chabal Y. J., "Controlled Deposition of Gold Nanoparticles on Well-Defined Organic Monolayer Grafted on Silicon Surfaces" *J. Phys. Chem. C* **2010**, *114*, 14180

[7] Peng, W., Seitz, O., Chapman, R. A., Vogel, E. M. & Chabal, Y. J. "Probing the intrinsic electrical properties of thin organic layers/semiconductor interfaces using an atomic-layer-deposited Al2O3 protective layer." *Appl. Phys. Lett.* **2012**, *101*, 051605

[8] Peng, W. N., DeBenedetti, W. J. I., Kim, S., Hines, M. A. & Chabal, Y. J. "Lowering the density of electronic defects on organic-functionalized Si(100) surfaces." *Appl. Phys. Lett.* **2014**, *104*, 241601.

[9] Seitz, O., Dai, M., Aguirre-Tostado, F. S., Wallace, R. M. and Chabal, Y. J. "Copper-Metal Deposition on Self Assembled Monolayer for Making Top Contacts in Molecular Electronic Devices" *J. Am. Chem. Soc.* **2009**, *131*, 18159-18167

[10] Royea, W. J., Juang, A. and Lewis, N. S. "Preparation of air-stable, low recombination velocity Si(111) surfaces through alkyl termination" *Appl. Phys. Lett.* **2000**, ***77***, 1988-1990

[11] De Benedetti W. J. I.; Nimmo M.T.; Rupich S. M.; Caillard L.M.; Gartstein Y. N.; Chabal Y.J. and Malko A.V., "Efficient Directed Energy Transfer through Size-Gradient Nanocrystal Layers into Silicon Substrates." *Adv. Funct. Mater.* **2014**, *24*, 5002-5010

[12] Huang, Z.; Geyer, N.; Werner, P.; de Boor, J.; Gösele, U.,"Metal-assisted chemical etching of silicon: a review" *Adv. Mater.* **2011,** *23*, 285-308.

[13] Brovelli S.; Shaller R.D.; Crooker S.A.; Garcia-Santamaria F.; Chen Y.; Viswanatha R.; Hollingsworth, J.A.; Htoon H.; and Klimov V. I., "Nano-engineered electron-hole exchange interaction controls exciton dynamics in core-shell semiconductor nanocrystals." *Nat. Comm.*, **2011**, *2*, 280

[14] Scott S.A.; Peng W. N.; Kiefer A.M; Jiang H.Q.; Knezevic I.; Savage D.E.; Eriksson M.A.; and Lagally M.G.," "Influence of Surface Chemical Modification on Charge Transport Properties in Ultrathin Silicon Membranes" *ACS Nano* **2009**, *3*, 1683

[15] Peng W.N; Aksamija Z.; Scott S.A; Endres J.J.; SavageD. E.; Knezevic I.; Eriksson M.A.; and Lagally M.G.," Probing Semiconductor Surface Electronic Structure with Charge Transport in Nanomembranes" *Nat. Commun.* **2013**, *4*, 1339

[16] Cui, Y., Wei, Q. Q., Park, H. K. & Lieber, C. M. "Nanowire nanosensors for highly sensitive and selective detection of biological and chemical species" *Science* **2001**, ***293***, 1289-1292

[17] S. M. Sze, *Physics of Semiconductor Devices* (John Wiley & Sons, Inc., 1981)

[18] Aberle A. G., "Surface passivation of crystalline silicon solar cells: a review", *Prog. Photovoltaics* **2000**, *8*, 473

[19] Nguyen, H. M.; Seitz, O.; Gartstein Y. N.; Chabal Y. J.; and Malko A. V., "Energy Transfer from Colloidal Nanocrystals into Si Substrates Studied via Photoluminescence Photon Counts and Decay Kinetics" *J. Opt. Soc. Am. B* **2013,** *30 (9)*, 2401-2408

[20] Nguyen, H. M.; Seitz, O.; Aureau D.; Sra A.; Nijem N.; Gartstein Y. N.; Chabal Y. J.; and Malko A. V., "Spectroscopic evidence for nonradiative energy transfer between colloidal CdSe/ZnS nanocrystals and functionalized silicon substrates" *Appl. Phys. Lett*., **2011**, *98*, 161904

[21] Nguyen, H. M.; Seitz, O.; Peng, W.; Gartstein, Y. N.; Chabal, Y. J.; Malko, A. V., Efficient Radiative and Nonradiative Energy Transfer from Proximal CdSe/ZnS Nanocrystals into Silicon Nanomembranes *ACS Nano*, **2012**, *6*, 5574

[22] Nimmo, M. T.; Caillard, L. M.; Benedetti, W. D.; Nguyen, H. M.; Seitz, O.; Gartstein, Y. N.; Chabal, Y. J.; Malko, A. V., Visible to Near Infrared Sensitization of Silicon Substrates via Energy Transfer from Proximal Nanocrystals: Further Insights for Hybrid Photovoltaics *ACS Nano*, **2013**, ***7***, 3236

[23] Shvarts D.; Haran A.; Benshafrut R.; Cahan D.; and Naaman R., "Monitoring electron redistribution in molecules during adsorption"*Chem. Phys. Lett.* **2002**, *354*, 349

[24] Costa-Fernandez, J. M; Pereiro, R.; Sanz-Medel, A, "The use of luminescent quantum dots for optical sensing", Trends in Analytical Chem., **2006**, ***25 (3)***, 207-218

[25] Yamamoto H.; Taniguchi K.; and Hamaguchi C.,"High-sensitivity SOI MOS Photodetector with Self-Amplification", *Jpn. J. Appl. Phys.* **1996**, *35*, 1382

[26] Seitz, O.; Caillard, L.; Nguyen, H. M.; Chiles, C.; Chabal, Y. J.; Malko, A. V., "Optimizing non-radiative energy transfer in hybrid colloidal-nanocrystal/silicon structures by controlled nanopillar architectures for future photovoltaic cells", *Appl. Phys. Lett*., **2012**, *100*, 021902